

# **Long-term Monitoring of Bacteria Undergoing Programmed Population Control in a Microchemostat**

## **Supporting Online Material**

### **Materials and Methods**

### **References and Notes**

### **Tables S1 & S2**

### **Figures S1-S5**

## **Materials and Methods**

**Microfluidic device design and fabrication:** The microchemostat chip was fabricated out of the silicone elastomer polydimethylsiloxane (PDMS) (General Electric RTV 615) using multi-layer soft lithography, as described previously (*SI*). Six reactors run in parallel on each chip.

**The microchemostat reader:** The reader consists of a Nikon TE 2000 (A. G. Heinze Inc., Lake Forest, CA) inverted microscope furnished with a PRIOR Scientific XYZ motorized stage system (A. G. Heinze Inc., Lake Forest, CA). Imaging was done using a Plan Fluor 40X 0.75NA ph2 DLL objective. The images were captured by a charge-coupled device (CCD) camera and digitized by a PXC200 color frame grabber (Cyberoptics Semiconductor, Beaverton, OR). We developed Labview software to control the synchronized operation of these components and all chip operation.

**Microscopic counting:** The microchemostat architecture is such that all the cells dwell in a chamber 10  $\mu\text{m}$  high, equivalent to the focal depth of the Plan Fluor 40X 0.75NA ph2 DLL objective. As such, the total number of cells in each continuous reactor was determined through automated microscopy by counting the number of cells present in a growth chamber section of known volume. A set of 8 still images was taken at a given location of each reactor, with rotary-mixing of the culture in between consecutive snapshots. We developed image-processing algorithms in Matlab to determine the average number of cells in each picture set, from which the reactor cell density was calculated. The motorized stage system enabled documentation of multiple simultaneous microchemostat experiments on a single chip.

**Active biofilm control:** The lysis buffer used was a bacterial protein extraction reagent (B-PER, Pierce, Rockford, IL).

**Media, strains and growth conditions:** Luria-Bertani (LB) medium contains 5g yeast extract, 10g tryptone and 10g NaCl per liter. LBK medium contains 10g tryptone, 5g yeast extract, and 7g KCl per liter, and 100mM 3-(N-morpholino) propanesulfonic acid (MOPS). MOPS EZ rich medium (TekNova Inc, Half Moon Bay, CA) contains 100ml of 10X MOPS, 10ml of 0.132M  $\text{K}_2\text{HPO}_4$ , and 100ml of 10X ACGU supplement and 580ml of 5X (amino acid) supplement EZ per liter. Medium pH (measured with Accumet® pH Meter 925, Fischer Scientific) was adjusted by adding 5M KOH.

*E. coli* strain MG1655 containing a low-copy number plasmid (pSC101 origin, kanamycin(R)) (S2) was received from Uri Alon (Figure 2). A revised version of the population control circuit (S3) on a single plasmid (Figure S1) was tested in MC4100Z1 cells (gift from Michael Elowitz) and Top10F' cells (Invitrogen). The MC4100Z1 strain

was constructed by inserting a cassette containing *lacIq*, *tetR*, and *spect(R)* genes into the chromosome of the MC4100 strain (genotype: *araD139*  $\Delta$ (*argF-lac*)205 *flb-5301* *pstF25* *rpsL150* *deoC1* *relA1*). We found that function of the single-plasmid version of the circuit was similar to that of the double-plasmid version. LB medium was used for cell growth to probe qualitative behavior and to prepare starter cultures for microchemostat experiments. To measure population control circuit dynamics, cells were grown in pH-buffered LBK medium. The population control circuit plasmid was maintained with 50  $\mu$ g/ml of kanamycin. When applicable, 1mM IPTG (unless otherwise stated) was used to activate the circuit. Under this condition, the circuit in MC4100Z1 is only *partially* induced due to the presence of the AraC repressor, which binds to the araO sites in the synthetic promoter (*S4*). However, we did not further induce the promoter using L-(+)-arabinose because it is toxic to the MC4100Z1 cells. 1mM IPTG can fully induce circuit function in Top10F' cells, because these cells do not produce AraC.

Precultures were prepared by inoculating a 2ml medium sample with cells from a single agar plate colony and shaking at 280rpm for 6 hours at 37°C. Each microchemostat culture was inoculated with a preculture sample to  $\sim$ 20 cells/nL. All microchemostat media were supplemented with 5g per liter bovine serum albumin as an anti-adhesion adjuvant. During experiments, the microchemostat chip was placed on a warming stage system (Brook Industries, Lake Villa, IL) to maintain growth temperature at  $\sim$ 32°C. Chip temperatures were monitored directly using a tip-sensitive thermocouple and an i/32 temperature monitoring system (Omega Engineering, Inc., Stamford, CT). The thermocouple was inserted into the chip through a vertical channel incorporated into the

chip PDMS structure to the cover slip floor of the chip beside the microchemostat reactors.

### **Biofilm formation in the absence of active biofilm control**

Without active biofilm control, biofilms always colonized the microreactor. Wall attachment of a single cell is followed by clonal growth and formation of sessile microcolonies that clog fluidic channels within 24-48 hours (Figure S2). Treatment of the microfluidic surfaces with non-adhesive surface coatings (such as poly (ethylene glycol) (PEG), ethylenediaminetetraacetic acid (EDTA), polyoxyethylene sorbitan monolaurate (Tween-20) and bovine serum albumin (BSA)) temporarily reduced adhesion but did not prevent biofilm growth. ‘Active biofilm control’ thoroughly thwarted all biofilm formation attempts for the entire range of experimental dilution rates ( $0.072 - 0.37 \text{ hr}^{-1}$ ) and over the lifetime of any given experiment. Every third ‘cleaning and dilution’ step was performed along the segment that housed the peristaltic pump to compensate for the additional adhesion resulting from the peristaltic pumping process.

### ***E. coli* growth in the microchemostat**

It has been shown that changes in pH and oxygen levels affect growth rates (S5). In experiments with the population control circuit, we used pH-buffered media to minimize the pH variation. Changes in oxygen concentration have been observed in other microfluidic bioreactors (S5), and they may have contributed to the small variations in the circuit OFF steady-state cell densities (Figures 2A, 3 & 4). Nevertheless, we expect variations in oxygen levels to be minor in our device because of the high gas permeability

of the PDMS, large surface area-to-volume ratio, and the continuous influx of fresh growth medium. In support of this notion, a recent study suggested that a reactor depth of 300 $\mu\text{m}$  (compared to a depth of 10  $\mu\text{m}$  of our device) would allow sufficient oxygenation to support  $10^9$  cells/ml (S6). We routinely obtained cell densities up to  $3 \times 10^9$  cells/ml, which strongly suggests that oxygen was not limiting growth.

### Modeling the population control circuit in the microchemostat

We revised a previous model to better capture the circuit dynamics:

$$\frac{dN}{dt} = N(k - D - kN / N_m) - dEN \quad (\text{Eq S1})$$

$$\frac{dE}{dt} = k_E R - d_E E \quad (\text{Eq S2})$$

$$\frac{dR}{dt} = k_R A - d_R R \quad (\text{Eq S3})$$

$$\frac{dA}{dt} = v_A N - (d_A + D)A \quad (\text{Eq S4})$$

$$D = -\frac{\ln[1 - F]}{T} \quad (\text{Eq S5})$$

where variables and parameters are described in detail in Tables S1 & S2. The dilution rate ( $D$ ) is related to two microchemostat operation parameters (Equation S5):  $T$  is the time interval (or periodicity) between each dilution event, during which a fraction  $F$  ( $\frac{1}{16}$ ) of the culture is exchanged. The only revision from previous version of the model (S3) is the introduction of an intermediate reaction step: activation of LuxR, which accounts for

the binding of the signal to the inactive LuxR, and dimerization of the active LuxR. Batch culture dynamics would correspond to the case where  $D = 0$ . If production and degradation of active LuxR are much faster than other reactions, we can reduce the above model to its previous form.

When  $N \ll N_m$ , equation S1 reduces to  $\frac{dN}{dt} = (k - D - dE)N$ . Then the simplified model will have two steady-state solutions:  $(N_s=0, E_s=0, R_s = 0, A_s=0)$  and  $(N_s = \frac{d_A d_E d_R k}{v_A k_E k_R d}, E_s = k/d, R_s = \frac{d_E k}{k_E d}, A_s = \frac{d_E d_R k}{k_E k_R d})$ . Based on linear stability analysis, the

trivial steady-state is always unstable. The non-trivial steady state is stable for:

$$(d_A + D)d_E d_R + ((d_A + D) + d_E + d_R)^2 (k - D) <$$

$$((d_A + D) + d_E + d_R)(d_E d_R + (d_A + D)(d_E + d_R))$$

From this inequality, we expect the systems to oscillate when degradation rates of LuxR, the killer protein, and the AHL signal, and the microchemostat dilution rates are all small enough. Increases in these parameters tend to stabilize the non-trivial steady state and diminish oscillation (Figure S3). The model could be further expanded to account for accumulation and washing-out of dead cells in the reactor. Numerical simulations indicate that the total cell density will only oscillate if the viable cell density oscillates.

## **Circuit function in macro-reactors**

Maintenance of circuit function in bulk cultures was ascertained as follows: at different time points after inoculation, samples were taken from each culture (ON or OFF) to measure viable cell density by serial dilution and plating. A significantly lower colony count for the ON cultures relative to their OFF counterparts indicated the presence of circuit function in the original culture at the point of plating. To further verify whether the apparent loss of circuit function was due to mutations, single colonies from some of these plates were re-tested in fresh media; these showed no recovery of circuit function. In general, the period for maintaining circuit function depends on the cell strain and growth conditions. MC4100Z1 cells lost circuit function within 72 hrs (Figure S4) and Top10F' within 48 hrs (Figure S5) in growth conditions and temperatures otherwise identical to those in the microchemostat.

## **Mutation rates**

On average, a mutant appears at a time proportional to  $1/(\mu N)$ , where  $N$  is the population size and is  $\mu$  the per-genome mutation rate. The time to fixation, on the other hand, is proportional to  $(2/s)*\ln(2N)$ , where  $s$  is the selective advantage (S7). Thus the rate at which a mutant with a large selective advantage, once it has appeared, will take over the population is expected to be higher (fixation time shorter) in a nanoscale reactor characterized by small total population size. We estimate that a rapidly-growing mutant will be detectable within 6-7 hours, while the underlying mutation process that leads to that mutant may be delayed many thousandfold in populations of hundreds to thousands of bacteria as opposed to macro-scale cultures

## References and Notes

- S1. T. Thorsen, S. J. Maerkl, S. R. Quake, *Science* **298**, 580-584 (2002).
- S2. M. Ronen, R. Rosengerg, B. Shraiman, U. Alon, *Proceedings of the National Academy of Sciences of the United States of America* **99**, 10555-10560 (2002).
- S3. L. C. You, R. S. Cox III, R. Weiss, F. H. Arnold, *Nature* **428**, 868-871 (2004).
- S4. R. Lutz, H. Bujard, *Nucleic acids research* **25**, 1203-1210 (1997).
- S5. N. Szita *et al.*, paper presented at the Micro Total Analysis Systems 2002, Nara, Japan 2002.
- S6. A. Zanzotto *et al.*, *Biotechnology and Bioengineering* **87**, 243-254 (2004).
- S7. W.-H. Li, *Molecular Evolution* (Sinauer Associates, Sunderland, MA, 1997)
- S8. R. Weiss, T. F. Knight, paper presented at the Proceedings of the Sixth International Meeting on DNA-Based Computers, Leiden, The Netherlands 2000.
- S9. C. H. Collins, F. H. Arnold, J. R. Leadbetter, *Molecular Microbiology* **55 (3)**, 712-723 (2004).
- S10. L. You, A. Hoonlor, J. Yin, *Bioinformatics* **19**, 435-436 (2003).

## Figure Captions

**Figure S1.** Implementation of the population control circuit (pPopCtrl1). The plasmid (p15A origin, kanamycin<sup>R</sup>) was verified by sequencing. It was constructed by inserting PCR-amplified p<sub>luxI</sub>-*lacZα-ccdB* (where *lacZα-ccdB* is the killer gene) from *pluxCcdB3* (S3) into plasmid pLuxRI between the AatII site. Plasmid pLuxRI was constructed by inserting PCR-amplified *luxI* from pSND-1 (S8) into pLuxR, downstream of *luxR* (S9). Note that the circuit is under control of a synthetic promoter p<sub>lac/ara-1</sub> (S4), and is inducible with IPTG.

**Figure S2.** (A-C) Optical micrographs of typical scenarios in the absence of active biofilm control depicting invading biofilms that stemmed from passive adhesion. In (C), two biofilms invading from either side of the growth chamber are about to osculate and clog the fluid channel. (D) A biofilm in-between the valves of a peristaltic pump initiated by affected adhesion. The scale bar is 100 μm long.

**Figure S3.** Typical simulation results for the population control dynamics inside the microchemostat. Initial conditions and parameter values are given in Tables S1 and S2 unless noted otherwise. The model generates sustained oscillations for a low microchemostat dilution rate ( $D=0.1 \text{ hr}^{-1}$ ) (blue), but damped oscillations when  $D$  is increased to  $0.3 \text{ hr}^{-1}$  (red). The numerical simulations were carried out using Dynetica (S10).

**Figure S4.** Growth of MC4100Z1 cells with the circuit ON (red triangles) or OFF (blue squares). Cells were grown in 4ml LBK MOPS (pH=7.6) at 32°C and shaking at 175 rpm. Viable cell densities were measured by serial dilution and plating. Shown data are the measurements from duplicate cultures, which demonstrated essentially the same behavior. It is evident from the growth curves that cells have lost circuit function by 72 hrs. Confirming this point, all 6 single colonies picked from the 72hr plates lost circuit function when re-tested in fresh media.

**Figure S5.** Growth of Top10F' cells with the circuit ON (red triangles) or OFF (blue squares). Cells were grown in 4ml LBK MOPS (pH = 7.0) at 32°C and shaking at 175 rpm. Cell densities were measured by serial dilution and plating. Shown data are the measurements from triplicate cultures, which demonstrated essentially the same behavior. It is evident from the growth curves that cells have lost circuit function by 48 hrs. Confirming this point, all 10 single colonies picked from the 48hr plates lost circuit function when re-tested in fresh media.

## Tables

**Table S1.** Model variables and their initial levels

Variables	Initial levels	Notes
N	$1 \times 10^7 \text{ ml}^{-1}$	Viable cell density
E	0 nM	LacZ $\alpha$ -CcdB concentration
R	0 nM	Dimerized, active LuxR concentration
A	0 nM	AHL concentration

**Table S2.** Model parameters and their base values

Parameters	Base values	Notes
$k$	$0.7 \text{ hr}^{-1}$	Maximum growth rate
$D$	$0.1 \text{ hr}^{-1}$	Dilution rate of the microchemostat
$N_m$	$3 \times 10^9 \text{ ml}^{-1}$	Carrying capacity of the medium
$d$	$0.004 \text{ nM}^{-1} \text{ hr}^{-1}$	Killing rate constant by LacZ $\alpha$ -CcdB
$k_E$	$1.0 \text{ hr}^{-1}$	Production rate constant of LacZ $\alpha$ -CcdB
$d_E$	$0.7 \text{ hr}^{-1}$	Decay rate constant of LacZ $\alpha$ -CcdB
$k_R$	$1.0 \text{ hr}^{-1}$	Production rate constant of active LuxR
$d_R$	$0.7 \text{ hr}^{-1}$	Decay rate constant of active LuxR
$v_A$	$4 \times 10^{-7} \text{ nM ml hr}^{-1}$	AHL synthesis rate constant
$d_A$	$0.1 \text{ hr}^{-1}$	Decay rate constant of AHL

Fig. S1

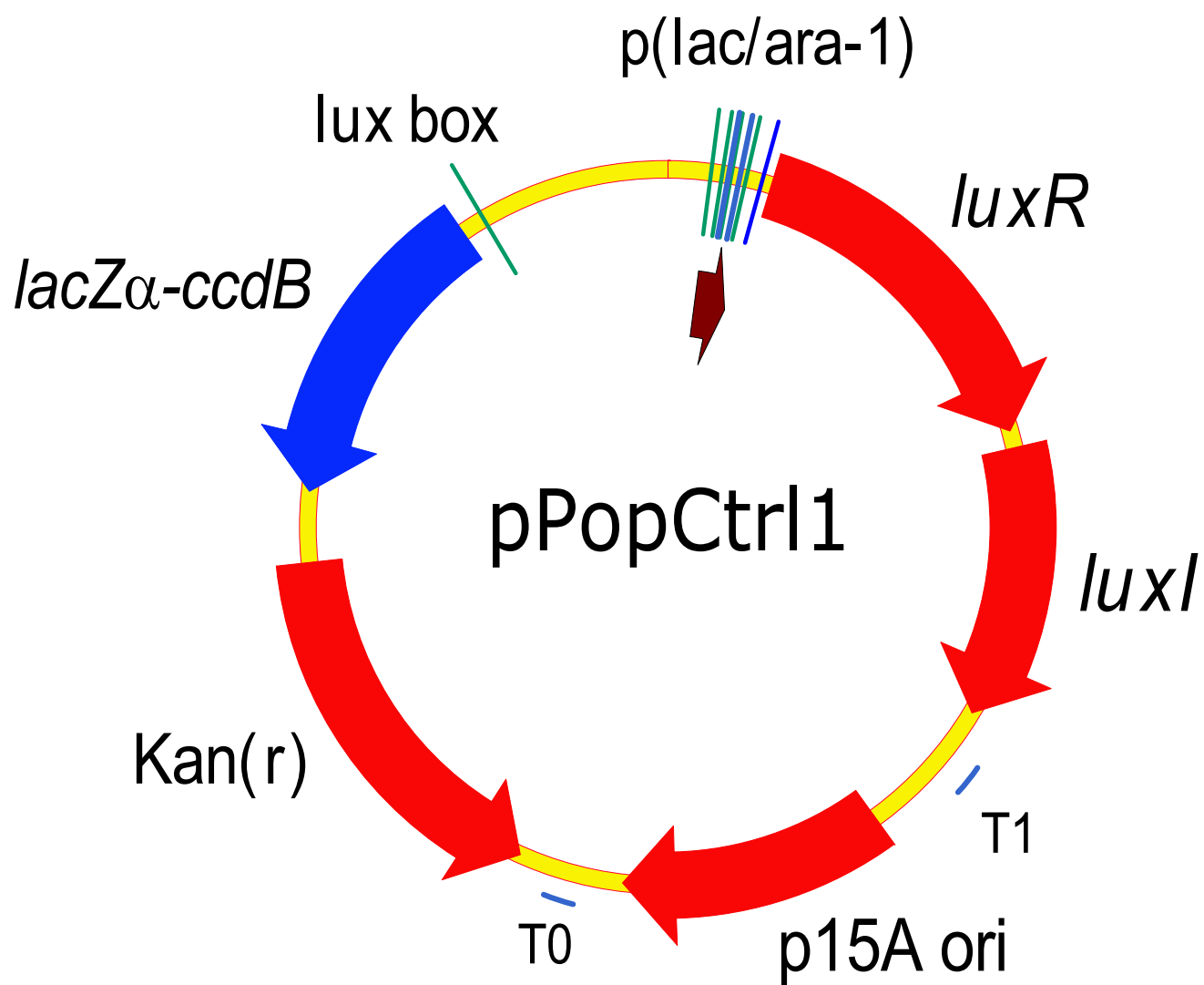


Fig. S2

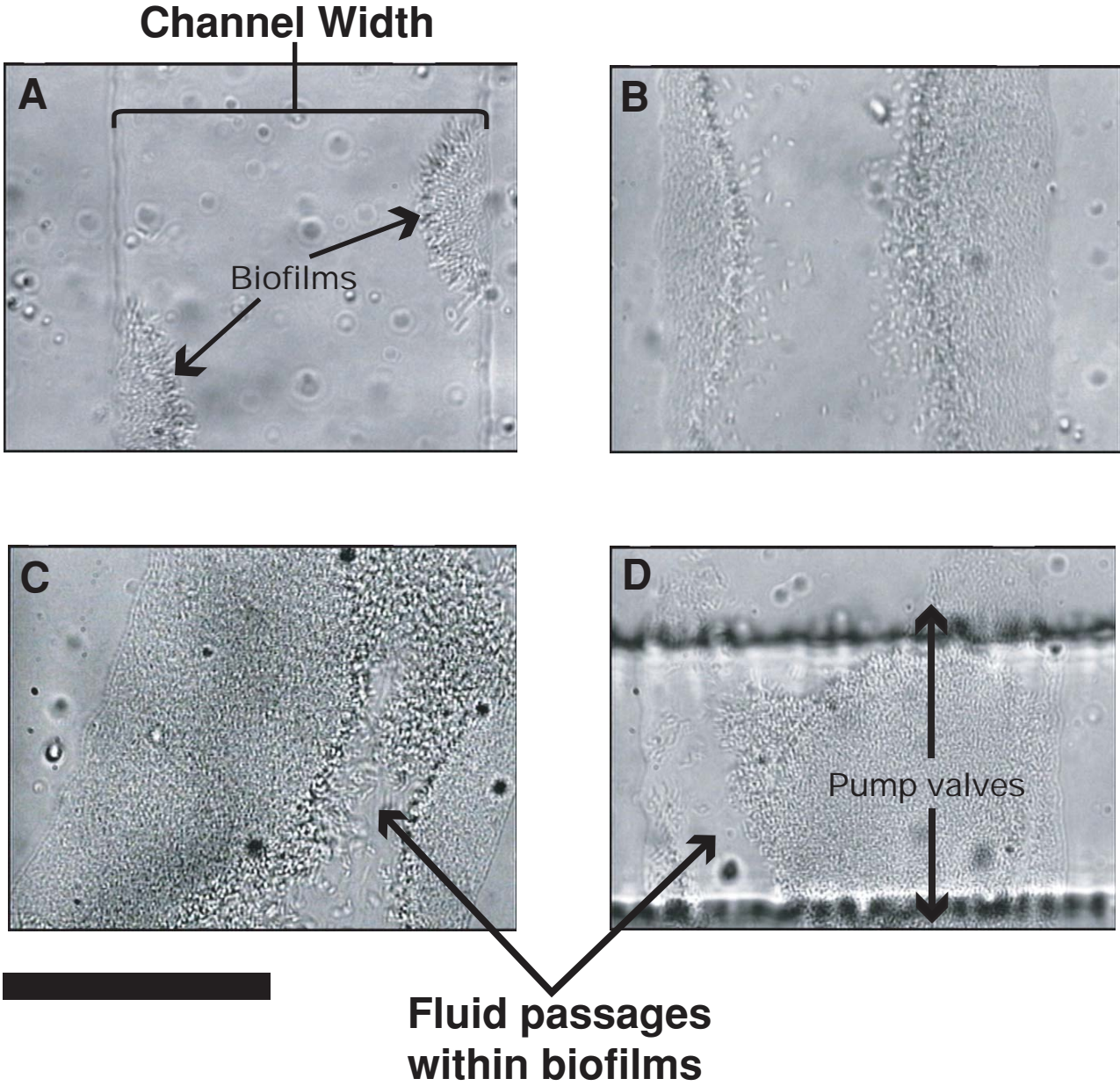


Fig. S3

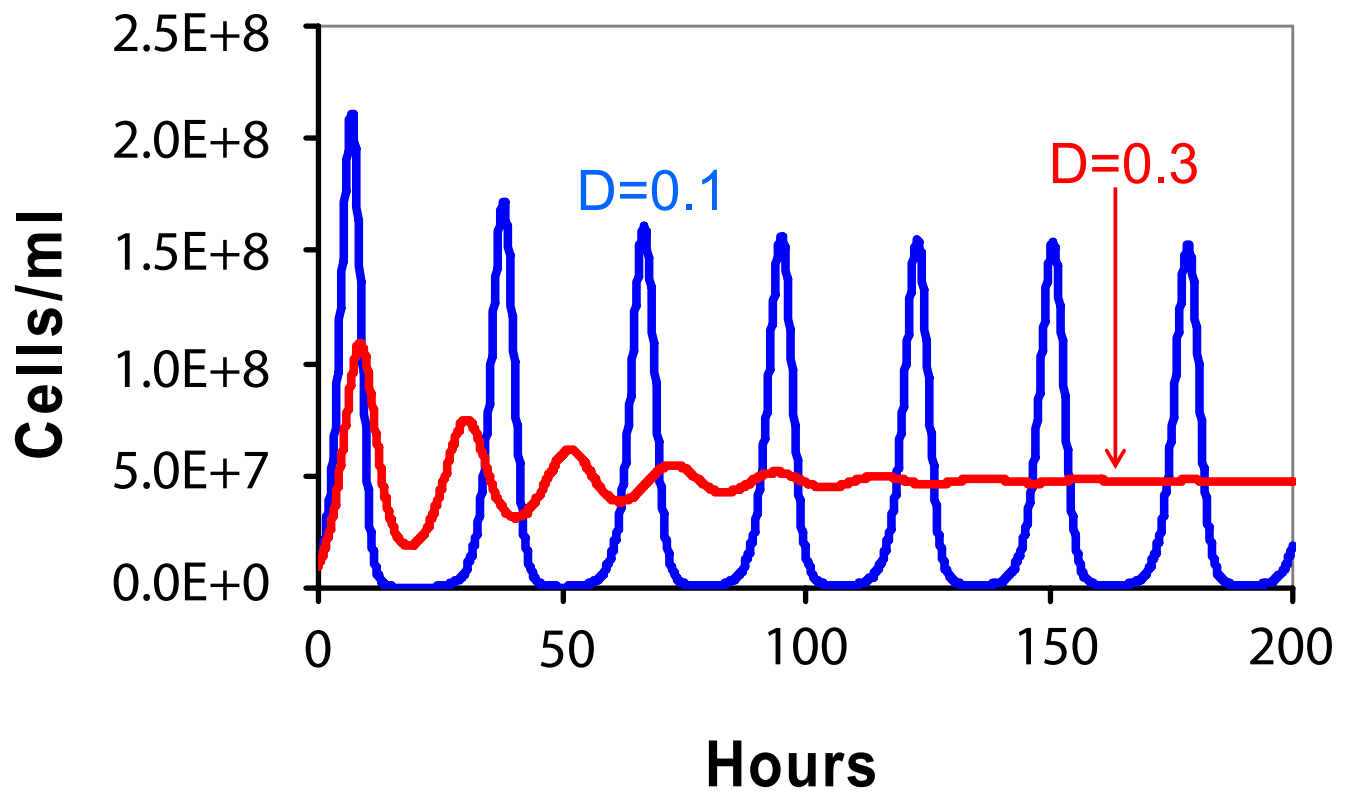


Fig. S4

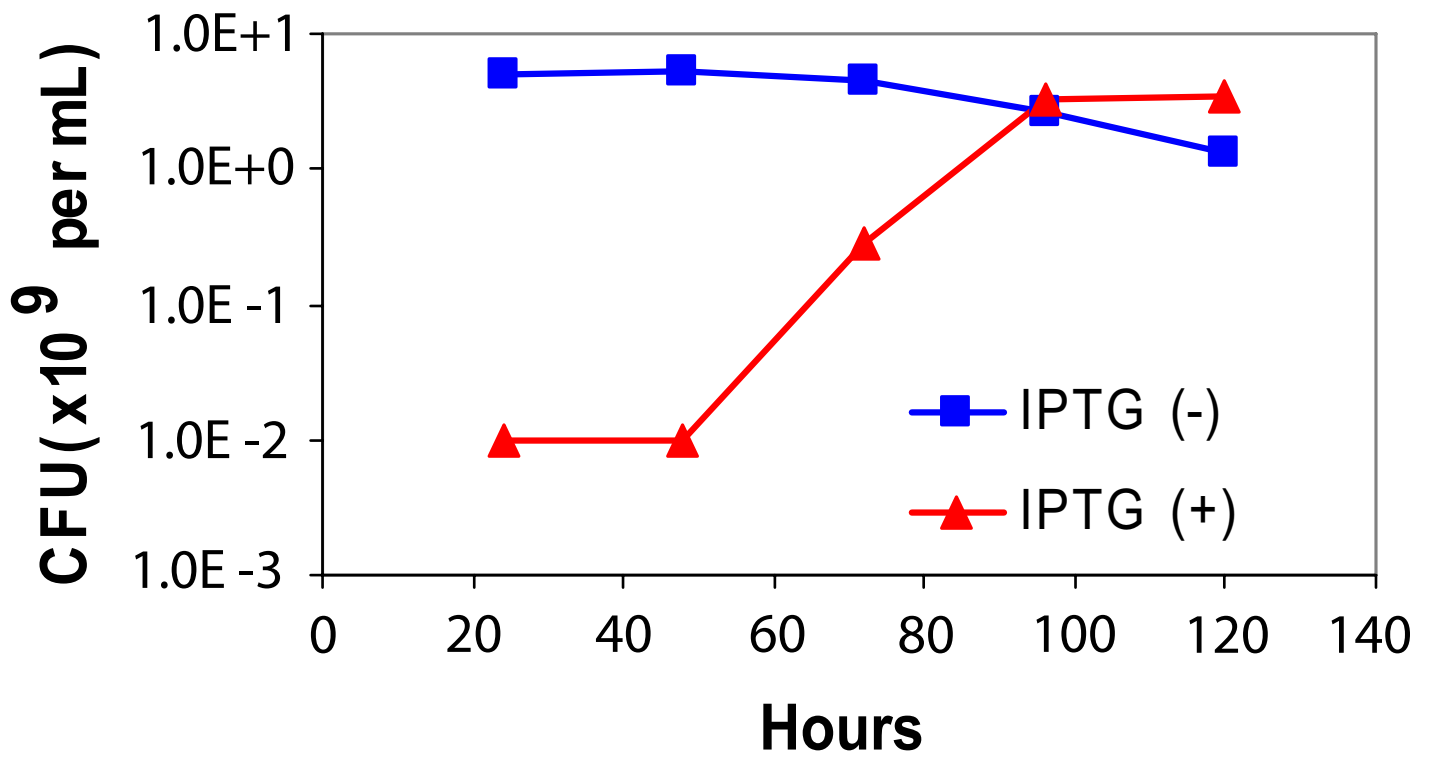


Fig. S5

